Interactions and transport in nanostructures

Bernhard Kramer, T. Brandes, Wolfgang Häusler, K. Jauregui, W. Pfaff, Dietmar Weinmann

Interactions and transport in nanostructures

B Kramer, T Brandes, W Häusler, K Jauregui, W Pfaff
and D Weinmann

I. Institut für Theoretische Physik, Universität Hamburg, Jungiusstrasse 9,
D-20355 Hamburg, Germany

Abstract. We discuss various aspects of electron–electron and electron–phonon interaction in electron transport in submicrometre structures. We show that it is only above a certain critical Fermi velocity that the acoustic phonons can significantly influence the electron states in a quasi-one-dimensional quantum wire. We predict a characteristic temperature dependence of the plateaus in the linear conductance as a function of a magnetic field which should be experimentally observable.

When the mean distance between Coulombically interacting electrons in a quantum dot is comparable to or larger than the Bohr radius their excitation spectrum shows fine structure which is related to the formation of a localized charge distribution, a Wigner molecule. We demonstrate that the excitations can be understood in terms of vibrational and tunnelling modes. Nonlinear transport of confined interacting electrons coupled to semi-infinite leads yields detailed information about the excitation spectrum. We present results including the degrees of freedom that were obtained from a master equation approach, and demonstrate that the correlations between the electrons lead to negative differential resistances that are related to spin selection rules.

1. Introduction

Interaction processes are of great importance for the understanding of the electronic transport properties of quantum coherent samples, although the conditions under which such a system can be considered as coherent depend strongly · on the *absence* of phase-breaking scattering. Among the many possibilities, electron–phonon (e–p) and electron–electron (e–e) interaction are most important [1]. In this contribution we discuss three aspects which demonstrate some most striking features in connection with electron transport in submicrometre structures.

First, we consider the interaction of acoustic phonons with the electrons in a quasi-one-dimensional quantum wire. We will demonstrate that it is only above a certain critical Fermi velocity that the phonons can influence the electron states significantly [2]. As a consequence, we predict a characteristic temperature dependence of the plateaus in the linear conductance as a function of a magnetic field which should be experimentally observable.

The Coulomb interaction between the electrons in a system that contains a quantum dot leads to rather sharp and regular resonance-like peaks in the linear conductance [3]. When the mean distance between the electrons in the dot is comparable to the Bohr radius (of the order of 10 nm for AlGaAs based heterostructures) the excitation spectrum of the interacting electrons shows fine structure which is related to the formation of a localized charge distribution, a Wigner molecule [4]. We show that the

excitation spectrum can be understood in terms of vibrational and tunnelling modes [5].

Nonlinear transport properties of interacting electrons in a quantum dot that is coupled to semi-infinite leads yield detailed information about the excitation spectrum. Using a master equation we present an investigation which includes also the spin degrees of freedom of the electrons [6, 7]. We demonstrate that correlations between the electrons lead to novel effects in the current. Negative differential resistances related to spin selection rules are predicted in accordance with recent experiments [8, 9]. Furthermore, asymmetric conductance peaks occur due to asymmetries in the coupling.

2. Acoustic phonon scattering in quantum wires

In very pure samples, e–e and e–p interaction remain the only scattering mechanisms of importance at low temperatures. We consider here scattering with acoustical phonons with speed of sound c_s. In quasi-one-dimensional (1D) 'metallic' electron systems based on semiconductor heterostructures the e–p interaction is qualitatively different from that in metals since in a quasi-1D subband the Fermi velocity can be made arbitrarily small, even smaller than the sound velocity, by carefully adjusting a magnetic field or a gate voltage.

We show that momentum and energy conservation lead to a crossover between two different e–p scattering regimes when the Fermi velocity v_F is tuned from small

to higher values and eventually becomes larger than c_S. A similar mechanism has been discussed some time ago in the context of the breakdown of the quantum Hall effect [10, 11]. In a quantum wire, the linear conductance Γ is determined by the scattering of incoming electrons [12] having Fermi velocity v_F. In ballistic transport the velocity does not affect the conductance, owing to a cancellation of v_F with the 1D density of states (DOS) up to a factor $2\pi\hbar$, leading to a quantization of Γ in units of e^2/h. When scattering occurs the value of v_F plays a crucial role for scattering rates, and therefore for the conductance itself.

The quantum wire is modelled in the x–y plane by using a parabolic confinement potential $V(y) = (1/2)m^*\omega_0^2 y^2$. A magnetic field B is assumed in the z direction. In the Landau gauge the eigenstates of the unperturbed system are

$$\Psi_{nk}(x) = \frac{1}{\sqrt{L}} \exp(ikx)\chi(z)\phi_{nk}(y) \qquad (1)$$

where ϕ_{nk} is the nth harmonic oscillator wavefunction displaced by $y_0 = -\hbar\omega_c/(m^*\omega_B^2)$ with effective magnetic length $l_B = (\hbar/m^*\omega_B)^{1/2}$. Here, $\omega_c = (eB/m^*c)$ is the cyclotron frequency (m^* effective electron mass) and $\omega_B = (\omega_0^2 + \omega_c^2)^{1/2}$. The corresponding energy dispersion is $\varepsilon_{nk} = \varepsilon_n + \gamma_B(\hbar^2/2m^*)k^2$ with $\gamma_B = (\omega_0/\omega_B)^2$ and $\varepsilon_n = (n + 1/2)\hbar\omega_B$. The factor γ_B can become much less than unity for strong magnetic fields.

We consider longitudinal acoustic phonons with frequency ω_Q and linear dispersion relation $\omega_Q = c_S|Q|$, Q being the 3D phonon wavevector. Optical phonons are not included. Their energy is too large to be important at the low temperatures considered here. We restrict ourselves to the lowest electronic subband $n = 0$.

The interaction Hamiltonian is

$$H_{e-p} = \frac{1}{\sqrt{\Omega}} \sum_{k,k',Q} V_Q M_{k,k'}(Q)c_k^\dagger c_{k'}(a_Q + a_{-Q}^\dagger) \qquad (2)$$

with matrix elements $M_{k,k'}(Q) = \langle k|\exp(ixQ)|k'\rangle$, and electron–phonon matrix elements $V_Q = D(\hbar Q/2\rho_M c_S)^{1/2}$. D denotes the deformation potential constant, ρ_M is the mass density and Ω the system volume.

Momentum conservation for the scattering of an electron from $|k\rangle$ to $|k'\rangle$ requires $Qe_x = k - k'$ and therefore $|Q| \geq |Qe_x| = |k - k'|$. Energy conservation yields $\gamma_B(\hbar/2m^*)|k^2 - k'^2| = c_S|Q| \geq c_S|k - k'|$, from which $\gamma_B(\hbar/2m^*)|k + k'| \geq c_S$ follows. For small momentum transfers we have $k \approx k'$, and we can evaluate the last inequality assuming $k \approx k_F$. It follows that $v_F \geq c_S$ is the condition for such a scattering event to take place.

We predict that the crossover mentioned above should be in principle observable in the two-point conductance of a quasi-ballistic quantum wire below about 1 K provided that e–p scattering is sufficiently significant at low temperatures. By tuning the Fermi velocity one can go from a region of exponentially small e–p scattering rates to a region with rates $\sim T^3$ which should lead to a corresponding decrease of the conductance plateau if $v_F > c_S$.

We assume the e–p interaction to be sufficiently weak to be treated by perturbation theory. In GaAs/AlGaAs this is certainly a good approximation. The electronic self-energy can be calculated by standard techniques to second order in V_Q. The imaginary part gives the inelastic lifetime of an electron of momentum k and energy ε

$$\tau^{-1}(\varepsilon, k) = \frac{2\pi}{\hbar\Omega} \sum_{Q,k} |V_Q|^2 |M_{k,k'}(Q)|^2$$

$$\times [(n_Q + f(\varepsilon_{k'}))\delta(\varepsilon - \varepsilon_{k'} + \hbar\omega_Q)$$

$$- (\omega_Q \to -\omega_Q)]. \qquad (3)$$

Here, n_Q denotes the Bose function for phonon frequency ω_Q and f the Fermi function with chemical potential μ. The terms in the square brackets correspond to phonon emission $(+\hbar\omega_Q)$ and absorption $(-\hbar\omega_Q)$, respectively.

Although electronic transport properties are described by the transport rate that has in general a different temperature dependence, the scattering rate τ^{-1} should reveal at least qualitatively the influence of e–p scattering [1]. If we found an exponentially small scattering rate we would conclude that the change of the conductance is also negligibly small. On the other hand, in the region where $\tau^{-1} \sim T^3$ we would expect a large influence on the conductance, though the quantitative T dependence might not be correct.

The matrix element $M_{k,k'}$ implies momentum conservation in the longitudinal (x) direction

$$|M_{k,k'}(Q)|^2 = \delta_{k,k'+Q_x}|\langle \chi\phi_{0k}|\exp(ix_\perp Q_\perp)|\chi\phi_{0k'}\rangle|^2 \qquad (4)$$

and reflects the fact that in the transverse direction the system is not translationally invariant.

Using the above definitions the scattering rate can be calculated. It consists of two contributions

$$\tau^{-1}(\varepsilon, k) = \tau_+^{-1}(\varepsilon, k) + \tau_-^{-1}(\varepsilon, k) \qquad (5)$$

where $\pm$ correspond to scattering to positive and negative values of the final momentum k_ω.

It is lengthy but straightforward to show that at low temperatures $k_B T \ll \varepsilon_F - \varepsilon_0$, and for $v_F > c_S$, $\tau_-^{-1}(\varepsilon_F) \sim T^3$ as for e–p scattering in metals. For $v_F < c_S$ only phonon absorption is possible and

$$\tau_+^{-1}(\varepsilon_F) \sim T \exp[-2(1 - v_F/c_S)\beta m^* c_S^2].$$

The rate τ_-^{-1} in this region is exponentially small, independent of the velocity ratio, so that the total scattering rate is essentially due to scatterings that do not cross the sample. Their efficiency in reducing the conductance Γ is less than that of backscattering across the wire. They nevertheless provide an important mechanism for breaking the phase coherence of the electrons which also leads to a reduction of Γ. In addition, in a strong magnetic field scattering across the wire is strongly suppressed by the exponential smallness of the corresponding matrix elements $M_{k,-k_\omega}$.

The crossover starts to get smeared out if $k_B T \approx \varepsilon_F - \varepsilon_0$. When the Fermi velocity is tuned by a gate voltage the temperature below which the effect is predicted to be observable at $v_F = c_S$ is given by $k_B T \approx (1/2)m^* c_S^2$. An estimate for GaAs with $m^* = 0.067m_e$ and $c_S = 5370$ m s^{-1}
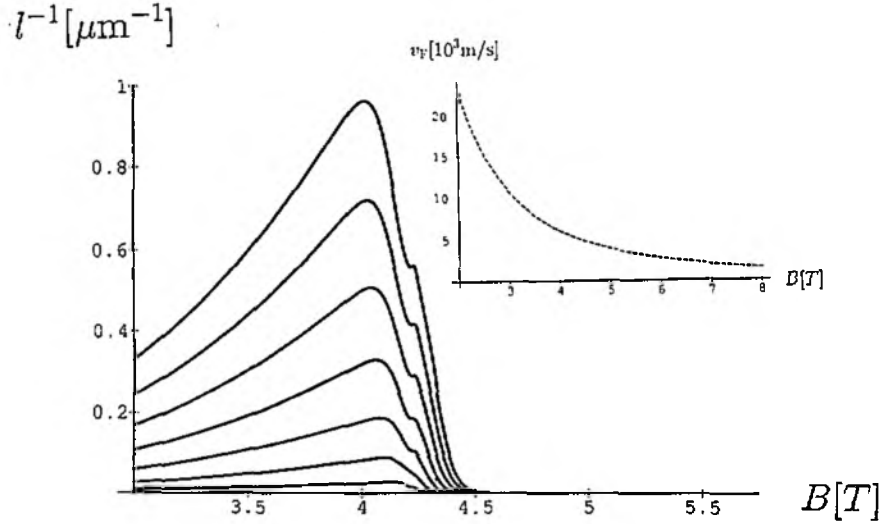
Figure 1. Inverse inelastic scattering length l^{-1} due to intraband e–p scattering in the lowest subband of a quantum wire in a magnetic field B. Temperatures are from 0.4 K to 1.6 K in steps of 0.2 K (from below), parameters were chosen with respect to a recent experiment [13] as $\hbar\omega_0 = 0.46$ meV and $n_L = 5 \times 10^8$ m^{-1}. Inset: Fermi velocity as a function of B.

yields $T = 64$ mK which is very low and might prevent the effect being observed here.

The situation is, however, drastically different if the Fermi velocity is tuned by a magnetic field [13]. For the parabolic confining potential one has $\varepsilon_F = \varepsilon_{k_F}$ with $k_F = (\pi/2)n_L$ and $v_F = \gamma_B(\hbar k_F/m^*)$, where n_L is the linear density of the electrons. Since $\varepsilon_F - \varepsilon_0 = (1/2\gamma_B)m^* v_F^2$ with $\gamma_B \ll 1$ depending on the strength of the confining potential and the B field, relatively large $\varepsilon_F - \varepsilon_0$ can yield quite low Fermi velocities. One can easily reach $v_F = c_S$ for $B \neq 0$, although the Fermi energy (which depends on the magnetic field) is relatively large.

Figure 1 shows the inverse scattering length $l^{-1} = [v_F\tau_+(\varepsilon_F)]^{-1}$ at different temperatures as a function of B for the lowest subband. The deformation potential D was assumed to be 13.5 eV, the mass density $\rho_M = 5.3$ g cm^{-3} and the speed of sound $c_S = 5370$ m s^{-1}. The wavefunction perpendicular to the 2DEG plane was assumed to be a Gaussian with an effective width of 100 Å. The results are not too sensitive to the precise value of this parameter. One clearly observes the onset of the scattering for $v_F > c_S$. At lower B, the inverse scattering length decreases because the DOS becomes smaller†.

3. Electron interaction in quantum dots

The importance of e–e scattering for transport in quantum wires is not yet very well established experimentally, although there are strong theoretical indications that interplay of e–e exchange interaction and confinement energy in strong magnetic fields determines whether or not the conductance is quantized [14] in terms of e^2/h or $2e^2/h$. On the other hand, there are strong

† Directly at the crossover the curves show a small shoulder. This is due to the fact that changing from phonon absorption to phonon emission, one passes through a region of zero-phonon DOS.
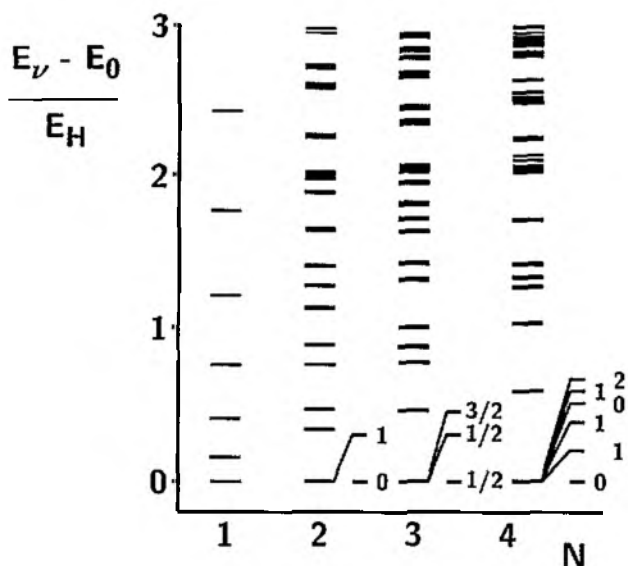
indications that Coulomb interactions are crucial for a thorough understanding of transport through quantum dots. For instance, periodic oscillations of the conductance through quantum dots that are weakly coupled to leads are well established consequences of the charging energy of single electrons entering or leaving the dot at sufficiently low temperatures [3].

To be specific we considered $N \leq 4$ interacting electrons in a quasi-1D square well of the length L including the spin degree of freedom [15]. We calculated numerically the exact eigenvalues E_v and the corresponding N-electron states $|v\rangle$ using the basis of Slater determinants. The Hilbert space was restricted to the M energetically lowest one-electron states. The interaction potential $\propto [(x - x')^2 + \lambda^2]^{-1/2}$ was used, where $\lambda (\ll L)$ is a parameter which simulates a transverse spread of the N-electron wavefunction. The Hamiltonian is

$$H = E_H \frac{a_B}{L}\left(\frac{a_B}{L} H_0 + H_i\right) \quad (6)$$

with the kinetic part

$$H_0 = \sum_{n,\sigma} \varepsilon_n c_{n,\sigma}^+ c_{n,\sigma} \quad (7)$$

($\varepsilon_n \approx n^2$, n integer), and the interaction energy

$$H_i = \sum_{m_1 \cdots m_4, \sigma_1, \sigma_2} V_{m_4 m_3 m_2 m_1} c_{m_4\sigma_1}^+ c_{m_3\sigma_2}^+ c_{m_2\sigma_2} c_{m_1\sigma_1}. \quad (8)$$

$E_H = e^2/a_B$ is the Hartree energy, $a_B = \varepsilon\hbar^2/m^* e^2$ the Bohr radius and ε the relative dielectric constant. The interaction matrix elements $V_{m_4 m_3 m_2 m_1}$ are real and do not depend on the spin state. Since the interaction is spin independent, the N-electron total spin S is a good quantum number. Figure 2 shows typical spectra for various N and $L = 9.45 a_B$.

For electron densities that are not too large a tendency towards Wigner crystallization is found (figure 3) [4]. In this regime, the excitation spectrum consists of

Figure 2. Energy spectra for different electron numbers for a system of length $9.45a_B$ in atomic energy units, E_H. Ground state energies E_0 are subtracted.
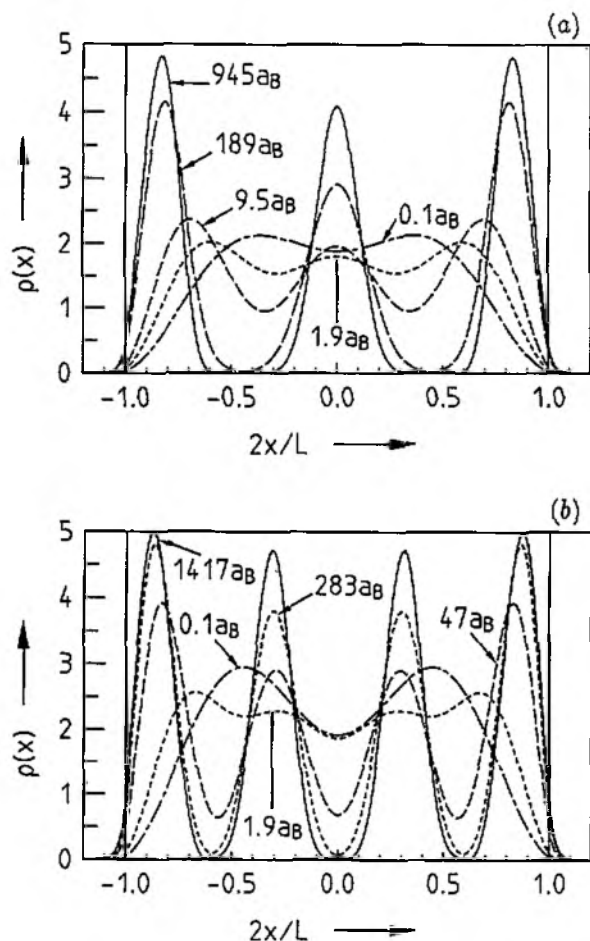

Figure 3. Charge density $\varrho(x)$ for $N = 3$ (a) and $N = 4$ (b) for different L ($0.1a_B \leq L \leq 1417a_B$, $M = 13$). The normalization is such that $\int dx \, \varrho(x) = N$. When $L \gtrsim 1a_B$ N peaks begin to emerge. For $L \gtrsim 100a_B$ the peaks are well separated.

well separated multiplets, each containing 2^N almost degenerate states [5]. The energetic differences between adjacent multiplets decrease according to a power law with electron density (figure 4). They correspond to
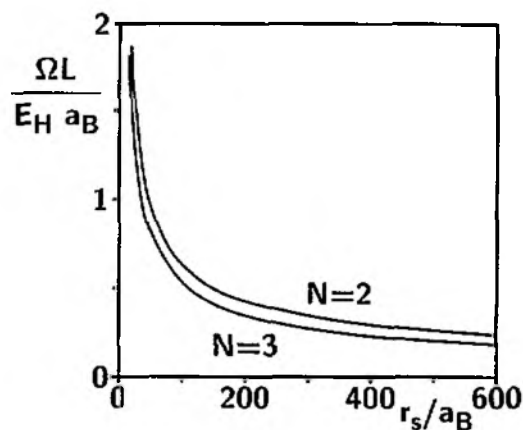

Figure 4. Energy difference between the two lowest multiplets, Ω, multiplied by L/a_B versus the mean particle distance r_s. Ω decreases more rapidly than $\sim r_s^{-1}$.
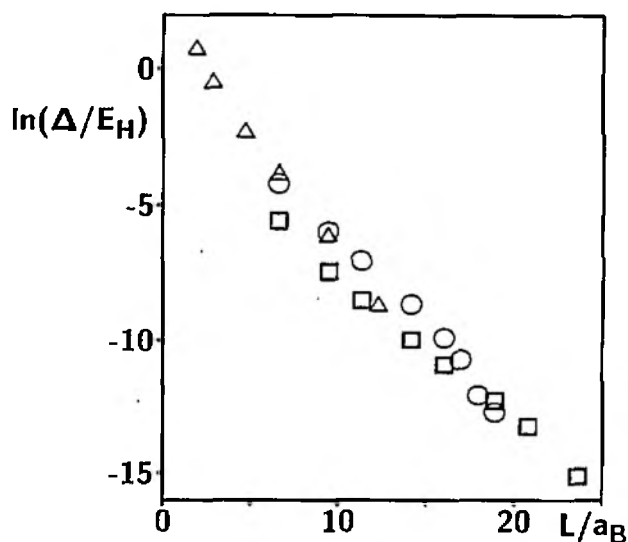

Figure 5. Logarithm of the energy difference Δ between the ground state and the first excited state within the lowest multiplet versus the system length for $N = 2$, $M = 11$ ($\square$), $N = 3$, $M = 13$ ($\bigcirc$) and $N = 4$, $M = 10$ ($\triangle$). The slope defines a critical mean electron distance of $1.5a_B$, which separates the non-interacting electron spectrum from the spectrum that is characteristic for the 1D interacting electron system.

vibrational excitations. At elevated electron densities the multiplets start to split exponentially (figure 5) revealing internal fine structure. Both types of excitation energies vary with diameter L of the sample, different from the L^{-2} behaviour of non-interacting electrons. The wavefunctions of individual levels within a given multiplet differ in symmetry and S. The internal structure of the level multiplets, which form the low-energy excitations of the correlated electron system, can be understood in terms of tunnelling between various arrangements of the separated electrons [16] (cf figure 3). A formulation in terms of localized, correlated many-electron wavefunctions, in contrast to the molecular field approximation, allows us to determine the fine structure spectrum analytically for $N \leq 4$ (table 1) and enormously simplifies calculations for larger N. Generalization to 2D situations

Table 1. Spin and energies of low-lying excitations of the correlated electron model at sufficiently large electron distances $r_s \equiv L/(n-1) \gg a_B$. The tunnelling integrals t_n decrease exponentially with r_s.

n	S	$E_v - E_0(N)$
2	0	0
2	1	$2t_2$
3	1/2	0
3	1/2	$2t_3$
3	3/2	$3t_3$
4	0	0
4	1	$(1 - \sqrt{2} + \sqrt{3})t_4$
4	1	$(1 + \sqrt{3})t_4$
4	0	$(2\sqrt{3})t_4$
4	1	$(1 + \sqrt{2} + \sqrt{3})t_4$
4	2	$(3 + \sqrt{3})t_4$

is possible and the agreement with numerical calculations is convincing. The different S of excited states should in principle be detectable by ESR and play a crucial role for nonlinear transport (section 4); the state with maximal spin $S = N/2$ is never the ground state. It can be shown that the ratios between the fine structure excitation energies are 'universally' independent of (not too high) electron densities and of the detailed form of the $e^- - e^-$ repulsion.

At bias voltages larger than the differences between discrete excitation energies within the dot, a characteristic splitting of the conductance peaks is observed [8, 9]. We will demonstrate unambiguously below that this is related to transport involving the excited states of N correlated electrons and that the shape of the peaks depends on the coupling between the quantum dot and the leads.

4. Coulomb and spin blockade effects

We consider the double-barrier Hamiltonian

$$H = H_l + H_r + H_D + H_l^T + H_r^T \qquad (9)$$

where $H_{l/r} = \sum_{k,\sigma} \varepsilon_k^{l/r} c_{l/r,k,\sigma}^+ c_{l/r,k,\sigma}$ describes free electrons in the left/right lead and

$$H_D = \sum_{m,\sigma} (\varepsilon_m - eV_G) c_{m,\sigma}^+ c_{m,\sigma}$$

$$+ \sum_{\substack{m_1, m_2, m_3, m_4, \\ \sigma_1, \sigma_2}} V_{m_1 m_2 m_3 m_4} c_{m_1, \sigma_1}^+ c_{m_2, \sigma_2}^+ c_{m_3 \sigma_2} c_{m_4, \sigma_1} \qquad (10)$$

the interacting electrons within the dot. The voltage V_G is the potential change in the dot due to an externally applied voltage and serves to change the electron density in the well.

The barriers are represented by the tunnelling Hamiltonians

$$H_{l/r}^T = \sum_{k,m,\sigma} (T_{k,m,\sigma}^{l/r} c_{l/r,k,\sigma}^+ c_{m,\sigma} + \text{HC}) \qquad (11)$$

where $T_{k,m,\sigma}^{l/r}$ are the transmission probability amplitudes which we assume to be independent of m and σ. We assume that the phase coherence between the eigenstates of H is destroyed within a time τ_Φ, on the average, which is much larger than the time an electron needs to travel from one barrier to the other. Thus, the motion of the electrons inside the dot is sufficiently coherent to guarantee the existence of quasi-discrete levels†. We assume also that the leads are in thermal equilibrium described by the Fermi–Dirac distributions $f_{l/r}(\varepsilon) = \{\exp[\beta(\varepsilon - \mu_{l/r})] + 1\}^{-1}$. The chemical potential in the left/right lead is $\mu_{l/r}$ and $\beta = 1/k_B T$ the inverse temperature. We assume the tunnelling rates through the barriers $t^{l/r} = (2\pi/\hbar) \sum_k |T_{k,m,\sigma}^{l/r}|^2 \delta(\varepsilon_k^{l/r} - E)$ to be independent of energy E. If they are small compared with the phase-breaking rate τ_Φ^{-1}, the time evolution of the occupation probabilities of the many-electron states in the dot can be calculated using a master equation [18–20]. We take into account the populations P_i of all possible Fock states $|i\rangle$ of H_D. Transitions between the latter occur when an electron tunnels through a barrier. Our method, which is based on the exact many-electron states of the dot including spin, allows us to determine the stationary non-equilibrium state without being restricted to the conventional charging model.

Each of the states $|i\rangle$ is associated with a certain electron number n_i, an energy eigenvalue E_i and the total spin S_i. For sufficiently small H^T, the transition rates between $|i\rangle$ and $|j\rangle$ with $N_i = N_j + 1$ are $\Gamma_{j,i}^{l/r,-}$ and $\Gamma_{i,j}^{l/r,+}$, depending on whether an electron is leaving or entering through the left/right barrier respectively. Here, $\Gamma_{j,i}^{l/r,-} = \gamma_{j,i} t^{l/r} (1 - f_{l/r}(E))$, $\Gamma_{i,j}^{l/r,+} = \gamma_{i,j} t^{l/r} f_{l/r}(E)$ and the electron provides the energy $E = E_i - E_j$. As an additional, and very important, selection rule we take into account that each added or removed electron can change the total spin S_i of the N_i electrons in the dot only by $\pm 1/2$. The consideration of the vector-coupling Clebsch–Gordan coefficients yields the spin-dependent factors

$$\gamma_{j,i} = \frac{S_i + 1}{2S_i + 1} \delta_{S_i + 1/2, S_j} + \frac{S_i}{2S_i + 1} \delta_{S_i - 1/2, S_j} \quad (12)$$

in the transition rates.

The master equation for the time evolution of the occupation probabilities P_i is

$$\frac{d}{dt} P_i = \sum_{j\,(j \neq i)} (\Gamma_{i,j} P_j - \Gamma_{j,i} P_i) \qquad \sum_i P_i = 1 \quad (13)$$

where $\Gamma_{i,j}$ are the elements of the matrix of the transition rates, $\Gamma = \Gamma^{l,+} + \Gamma^{r,+} + \Gamma^{l,-} + \Gamma^{r,-}$. From the stationary solution $\{\bar{P}_i\}$, which is obtained by putting $dP_i/dt = 0$ in (13) the DC current, the number of electrons that pass the left/right barrier per unit of time, is determined

$$I \equiv I^{l/r} = \mp e \sum_{i,j\,(j \neq i)} \bar{P}_j(\Gamma_{i,j}^{l/r,-} - \Gamma_{i,j}^{l/r,+}).$$

† It is well known that strong dissipation can suppress tunnelling [17]. This choice for the phase-breaking rate τ_Φ^{-1} guarantees that the renormalization of the tunnelling rates through the barriers is negligible.
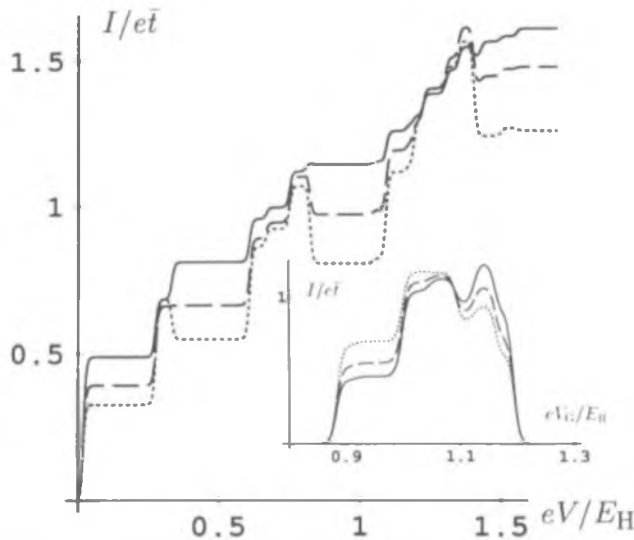
Figure 6. Current–voltage characteristics ($\mu_r = 0$) and the splitting of the fourth conductance peak at $\mu_1 = 0.3E_H$ and $\mu_r = 0$ (inset) of a dot of length $L = 15a_B$ described by the correlated electron model for $\beta = 200/E_H$. Tunnelling integrals are $t_2 = 0.03E_H$, $t_3 = 0.07E_H$ and $t_4 = 0.09E_H$, numerically determined ground state energies $E_0(1) = 0.023E_H$, $E_0(2) = 0.30E_H$, $E_0(3) = 0.97E_H$, $E_0(4) = 2.15E_H$. Broken, dotted and full curves correspond to $t^l/t^r = 1$, 2 and 0.5 respectively. The current is plotted in units of the total transmission rate $\bar{t} = t^l t^r/(t^l + t^r)$.

Figure 7. Grey scale plot of the differential conductance as a function of the gate voltage and the transport voltage. Negative differential conductances are indicated by light regions.

Figure 8. The most prominent feature in figure 6 for $t^l > t^r$ is magnified (dotted curve, in units of $e\bar{t}$), and the corresponding populations of the most relevant dot states **a**: $N = 2$, $S = 0$, **b**: $N = 2$, $S = 1$, **c**: $N = 3$, $S = 1/2$ (ground state), **d**: $N = 3$, $S = 1/2$ (first excited state), **e**: $N = 3$, $S = 3/2$ versus bias voltage V. Decreasing current is accompanied by an increase of the population of the spin polarized $N = 3$, $S = 3/2$ state at the expense of the other populations.

Current–voltage characteristics and conductivity peaks calculated by using the excitation energies given in table 1 are shown in figure 6 for temperatures lower than the excitation energies. We observe fine structure in the Coulomb staircase consistent with recent experiments [8, 9], and earlier theoretical predictions using a different approach [18, 19]. Within our model, the Coulomb steps are not of equal length as in the phenomenological charging model used previously [18]. This deviation from the classical behaviour is related to the inhomogeneity of the quantum mechanical charge density of the ground state [4, 15]. The heights of the fine structure steps are more random due to the non-regular sequence of total spins (cf table 1) and the spin selection rules. In certain cases, fine structure steps in the $I–V$ characteristic may even be completely suppressed.

Strikingly, regions of negative differential conductance occur (figures 6 and 7). They are related to the reduced probability for the states with maximal spin, $S = N/2$, to decay into states with lower electron number. In contrast to transitions that involve $S < N/2$ they are only possible if S is reduced. The corresponding Clebsch–Gordan coefficients are smaller than those for transitions with increasing S (cf equation (12)) which leads to an additional reduction of the current as compared with the situation where $S < N/2$. When the voltage is raised to such a value that an $S = N/2$ state becomes involved in the transport, this state attracts considerable stationary population at the expense of the better conducting $S < N/2$ states, as can be seen in figure 8.† Both effects
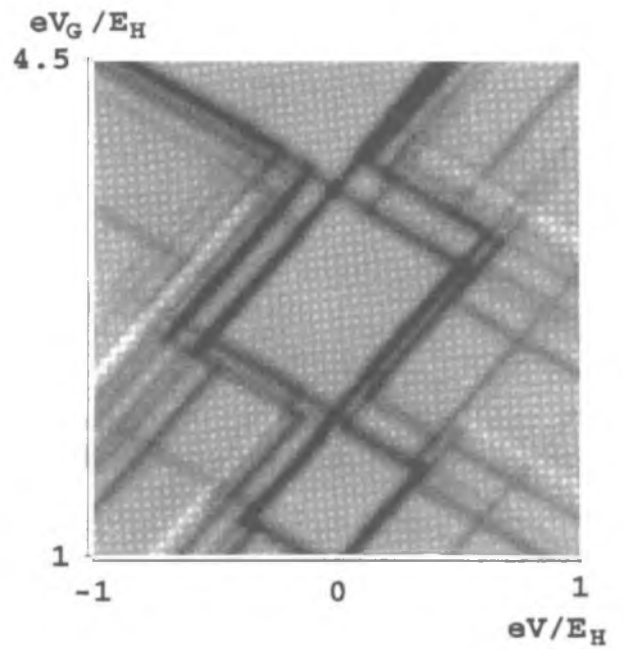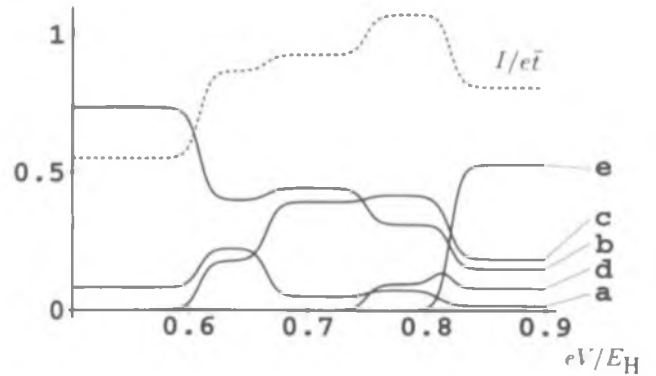
together can then add up to a decreasing current. The decrease in the $I–V$ curve becomes less pronounced if $t^l < t^r$, because then the dot is mostly empty and the $(N-1) \to N$ transitions determine the current. On the other hand if $t^l > t^r$ the *spin blockade* becomes more pronounced, because the $N \to (N-1)$ transitions limit the current in this case. Both features can be observed in figure 6 and also the experimental data of [8, 9] are clearly consistent with an interpretation that the potential barriers are slightly different. Negative differential conductances can in principle be used to construct a mesoscopic oscillator.

† The populations shown here do not sum up to unity because of the occupation of other states.

For low V, the conductance shows peaks when V_G is varied, which can be described within thermal equilibrium in the limit of linear response [21]. Only the (correlated N-electron) ground states are involved at zero temperature. For finite bias voltages, $eV = \mu_l - \mu_r$, larger than the level spacing, a varying number of levels contribute to the current when V_G is changed. The conductance peaks split and show structure as is observed experimentally and explained qualitatively in [8, 22] within the charging model. Asymmetric coupling to the leads changes the shape of the peaks considerably, as can be seen in figure 6. We propose to explain the 'inclination' of the conductance peaks observed in the experiment [8, 9] by asymmetric barriers and predict that this inclination will be reversed if the sign of the bias voltage is changed. Such asymmetric conductance properties can be used to construct mesoscopic rectifiers. Similar effects were inferred earlier from the high-frequency properties of mesoscopic systems containing asymmetric disorder [23].

dots', are, however, necessary to clarify the quantitative aspects.

'Preliminary' results taking into account a magnetic field in the direction of the transport show that the negative differential conductance is influenced and suppressed at high fields. To clarify these questions and to be able to make quantitative comparison with existing experiments data, generalization of the above correlated electron model to 2D is necessary.

Acknowledgments

5. Conclusions

In summary, we predict a reduction of the conductance plateaus for quantum wires due to an onset of acoustical phonon scattering at low temperatures for $v_F > c_S$ well below the onset of a new conductance plateau. The underlying physics can be understood using energy and momentum conservation. It should be observable in a characteristic decrease of the conductance at Fermi energy and/or magnetic fields that correspond to $v_F > c_S$ when the temperature is increased. This is in contrast to the temperature-dependent smearing of disorder-induced antiresonances at the onset of a new plateau, which would lead to an increase of the conductance with increasing temperature.

Furthermore, it is shown that correlations in semi-conducting quantum dots qualitatively influence the spectrum and its variation with dot diameter. The lowest excitation energies involve spin and can be understood through the inhomogeneous charge density distribution. Their ratios are not sensitive to the form of the e^--e^- repulsion.

The Coulomb and spin effects lead to conventional Coulomb blockade and a novel spin blockade effect in nonlinear transport through a double barrier. Most strikingly, regions of negative differential conductance occur because for each electron number the state of maximum spin can only contribute to transport by reducing the total spin. As a consequence, the transition probability into states with lower electron number is reduced. Spin blockade is not restricted to the quasi-1D model considered here but should also occur in 2D systems used in the experiments as long as the density of the electrons is sufficiently small.

All of the theoretically predicted features described above are qualitatively consistent with experiment [8, 9]. Further experiments, in particular using 'slim quantum

References

[1] For a general discussion of dephasing and inelastic scattering, see Stern A, Aharonov Y and Imry Y 1990 *Phys. Rev.* A **41** 3436
Imry Y and Stern A 1994 *Semicond. Sci. Technol.* **9** 1879
[2] Brandes T and Kramer B 1993 *Solid State Commun.* **88** 773
[3] Meirav U, Kastner M A and Wind S J 1990 *Phys. Rev. Lett.* **65** 771
Kastner M A 1992 *Rev. Mod. Phys.* **64** 849
[4] Jauregui K, Häusler W and Kramer B 1993 *Europhys. Lett.* **24** 581
Brandes T, Jauregui K, Häusler W, Kramer B and Weinmann D 1993 *Physica* B **189** 16
[5] Häusler W and Kramer B 1993 *Phys. Rev.* B **47** 16353
[6] Häusler W, Jauregui K, Weinmann D, Brandes T and Kramer B 1994 *Physica* B **194–196** 1325
[7] Weinmann D, Häusler W, Pfaff W, Kramer B and Weiss U 1994 *Europhys. Lett.* **26** 467
[8] Johnson A T, Kouwenhoven L P, de Jong W, van der Vaart N C, Harmans C J P M and Foxon C T 1992 *Phys. Rev. Lett.* **69** 1592
[9] Weis J, Haug R J, von Klitzing K and Ploog K 1993 *Phys. Rev. Lett.* **71** 4019; 1992 *Phys. Rev.* B **46** 12837
[10] Heinonen O, Taylor P L and Girvin S M 1984 *Phys. Rev.* B **30** 3016
[11] Středa P and von Klitzing K 1984 *J. Phys. C: Solid State Phys.* **17** L483
[12] Landauer R 1970 *Phil. Mag.* **21** 863
Büttiker M 1986 *Phys. Rev. Lett.* **57** 1761
[13] Wróbel J, Kuchar F, Ismail K, Lee K Y, Nickel H, Schlapp W, Grabecki G and Dietl T 1993 *10th Int. Conf. on Electronic Properties of Two-Dimensional Systems (Newport, 1993)*
[14] Kinaret J M and Lee P A 1990 *Phys. Rev.* B **42** 11768
[15] Häusler W, Kramer B and Mašek J 1991 *Z. Phys.* B **85** 435
[16] Häusler W 1994 *Preprint*
[17] Weiss U 1993 *Quantum Dissipative Systems (Series in Modern Condensed Matter Physics, vol 2)* (Singapore: World Scientific)

[18] Averin D V and Korotkov A N 1990 *J. Low Temp. Phys.* **80** 173

[19] Averin D V, Korotkov A N and Likharev K K 1991 *Phys. Rev.* B **44** 6199

[20] Beenakker C W J 1991 *Phys. Rev.* B **44** 1646

[21] Meir Y, Wingreen N S and Lee P A 1991 *Phys. Rev. Lett* **66** 3048

[22] Foxman E B, McEuen P L, Meirav U, Wingreen N S, Meir Y, Belk P A, Belk N R, Kastner M A and Wind S J 1993 *Phys. Rev.* B **47** 10020

[23] Fal'ko V I 1989 *Europhys. Lett.* **8** 785